

# BUILDING LANE-LEVEL MAPS FROM AERIAL IMAGES

Jiawei Yao<sup>1\*</sup> Xiaochao Pan<sup>2\*</sup> Tong Wu<sup>1</sup> Xiaofeng Zhang<sup>3</sup>

<sup>1</sup> University of Washington <sup>2</sup> Taiyuan University of Technology  
<sup>3</sup> Shanghai Jiao Tong University

## ABSTRACT

Detecting lane lines from sensors is becoming an increasingly significant part of autonomous driving systems. However, less development has been made on high-definition lane-level mapping based on aerial images, which could automatically build and update offline maps for auto-driving systems. To this end, our work focuses on extracting fine-level detailed lane lines together with their topological structures. This task is challenging since it requires large amounts of data covering different lane types, terrain and regions. In this paper, we introduce for the first time a large-scale aerial image dataset built for lane detection, with high-quality polyline lane annotations on high-resolution images of around 80 kilometers of road. Moreover, we developed a baseline deep learning lane detection method from aerial images, called AerialLaneNet, consisting of two stages. The first stage is to produce coarse-grained results at point level, and the second stage exploits the coarse-grained results and feature to perform the vertex-matching task, producing fine-grained lanes with topology. The experiments show our approach achieves significant improvement compared with the state-of-the-art methods on our new dataset. Our code and new dataset are available at <https://github.com/Jiawei-Yao0812/AerialLaneNet>.

**Index Terms**— Computer Vision, Lane Detection, Remote Sensing

## 1. INTRODUCTION

The rapid development of intelligent technology [1, 2, 3, 4] has led to heavy application of HD mapping techniques in intelligent transportation systems, particularly in the context of autonomous driving. The perception of the environment surrounding the autonomous vehicle is the most fundamental and important technology [5, 6, 7], including many challenging tasks [8], like lane detection, object detection [9] and depth estimation [10]. Among them, lane detection is the basic and essential task, whose detection results may affect driving performance and personal safety.

Recently, some researchers introduced deep-learning based method to build road maps from sensor data. Generally, previous methods focus more on performing online lane detection from vehicle’s egocentric sensor data and use

for planning [11, 12], or building a coarse-level map of the road network or curb map [13, 14]. However, building detailed lane maps offline from top-view aerial image data is feasible but not under-studied, and the accuracy and effectiveness of such high-definition mapping are still significantly underperformed. There is a lack of a benchmark and baseline for offline lane recognition from aerial images task.

Previous lane detection datasets such as SDLane [15], ONCE-3DLanes [16], and OpenLane [17] are all designed for lane detection from a vehicle perspective. In this paper, we introduce a new benchmark for lane detection using aerial images. This benchmark covers various areas and includes different lane types with high-quality labeling and high-resolution images. The dataset contains 7,763 images and over 150,000 lanes covering different lane standards, terrain and regions, providing a comprehensive resource for researchers in this field.

We also propose a baseline method of building accurate lane maps offline from aerial images. Specifically, we developed a two-stage cascaded lane detection approach called AerialLaneNet, in which the first stage is responsible for producing coarse-grained results and features, and the second stage fully exploits the coarse-grained results and feature maps to perform the vertex matching task and produce fine-grained results at the instance level. The main contribution of this work can be summarized as follows: (1) We present the first-ever benchmark for lane detection from aerial images covering different areas and various lane types with high-quality labeling and high-resolution images. This benchmark can facilitate research in this field. (2) We propose a novel cascaded lane detection approach using aerial images, called AerialLaneNet, which consists of two cascaded stages refining the results from point level to instance level. (3) Comprehensive experiments demonstrated that our method has outstanding performance in comparison with state-of-the-art methods.

## 2. AERIAL LANE (AEL) DATASET

### 2.1. Overview

Our work aims to build a benchmark and baseline for detecting vectorized lane lines from high-resolution aerial images. Compared to previous techniques such as detecting dy-

\* These authors contributed equally to this work.

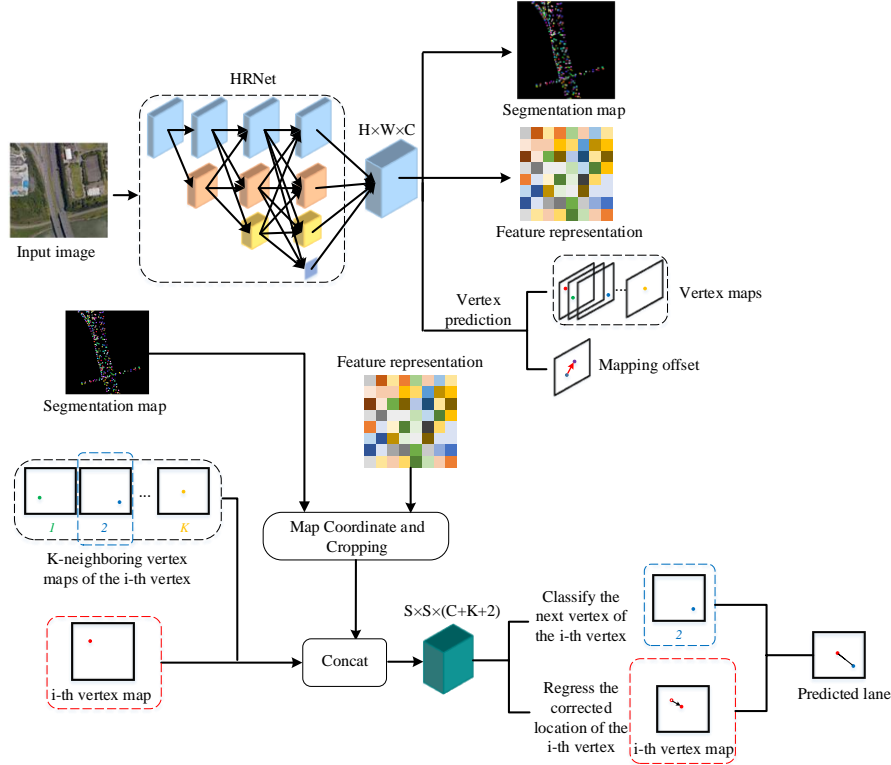


**Fig. 1.** Overview of our proposed method AerialLaneNet composed of the first stage: predicting segmentation map, feature map and vertex maps. The second stage takes previous stage as input and predicts each of the next vertex to link the vertices as polyline.

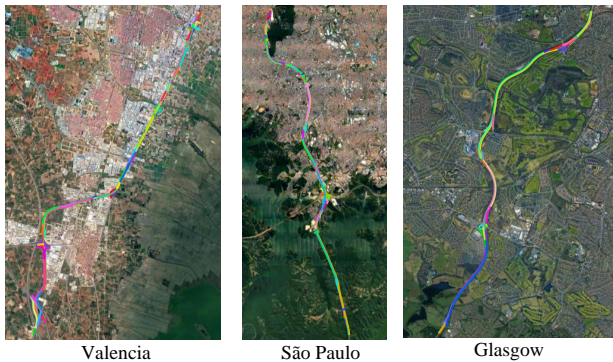


**Fig. 2.** Three of the annotated region in AEL dataset. Our dataset comprises images from various regions, backgrounds, lane types, topologies, and colors, making the lane detection task challenging.

dynamic lane maps from ego-vehicle view and road network or curb detection techniques, our task generates accurate lanes as polylines as offline maps for autonomous driving systems to leverage in planning and navigation. Therefore, we propose the Aerial Lane (AEL) Dataset, which is the first aerial image dataset with lane-level annotations to our knowledge. The source of images is from Google Map service [18] and we exploit QGIS [19] to label the lane lines. We will intro-

duce in this section the specification and statistics for the AEL dataset.

## 2.2. Annotation Specification

We directly labeled polylines as the lane lines and the vertices are stored in the form of latitude and longitude coordinates, which makes the dataset easier to share and update. In order to connect vertices into polylines, the direction of the edge is the same in each polyline. In labeling the dataset, the criteria for placing vertex is that the polylines connected by adjacent vertex should approximate the lane line as much as possible, given that the lane lines are actually curves.

To record the attributes of each lane line in detail, we identify 3 attributes of lanes: single or double line, white or yellow line, solid or dash line. Apart from lane attributes, we record the road\_id that each lane line belongs to, and also assign each lane an id. After annotating the dataset, we export image patches together with the corresponding lane annotation JSON file, the lane mask image from QGIS. We exported images at various heights at random region, and the resolution of every image is  $1280 \times 1280$ .

## 2.3. Dataset Statistics

Firstly, we chose 11 regions, and each region consists of a road between 3 and 27 kilometers long with various back-

Region	Number of Lanes	Number of Vertices	Total Length (KM)
Cairo	240	2495	3.721
Aucamville	130	4534	17.815
San Paulo	779	14811	26.563
Nevada	29	1134	6.414
Gopeng	13	1011	4.179
Glasgow	157	4428	9.203
Valencia	434	7116	12.044

**Table 1.** The statistics of the AEL dataset, containing the number of lanes, number of vertices, and total road length of each region.

grounds and terrain such as desert by the coastline in Dubai, urban area of Valencia and forest region in Perak State. Table 1 shows the statistics about the annotated lanes with respect to different regions.

We then export from QGIS 7,763 images together with over 150,000 lane lines in the form of pixel coordinates for training and evaluating the neural network. Our split ratio of training set:validation set:test set is 7:2:1. Figure 2 demonstrates a few sample images from our proposed dataset.

### 3. THE PROPOSED BASELINE: AERIALLANENET

Figure 1 illustrates overall architecture of proposed method, which consists of two stages. The first stage is designed to extract feature representation, and predict the lane segmentation map and vertex maps. In the second stage, each vertex is matched with its next vertex based on the segmentation map, feature representation and vertex maps from stage one.

For the segmentation branch in the first stage, we adopt HRNet [24] as the backbone network to provide high-resolution representation for image segmentation. With the lane segmentation and high-resolution features at hand, our approach further achieves instance-level lane lines in two steps. Firstly, the feature representation learns lane position information from the segmentation task and is used to predict vertex maps. Next, we will introduce in detail vertex matching using the results produced in the first stage (feature representation, segmentation map, and vertex maps) to obtain instance-level lane lines.

#### 3.1. Vertex Prediction

We predict vertex maps  $\hat{Y} \in [0, 1]$  with the size  $H \times W \times C$ , where  $H$  and  $W$  denote height and width of vertex maps, respectively, and  $C$  represents the max vertex number, which is set to the max vertex number of an image in the dataset. Specifically,  $\hat{Y}_{x,y,c} = 1$  represents a detected vertex, and  $\hat{Y}_{x,y,c} = 0$  denotes the background.

The vertex prediction process is similar to [25]. For each ground truth  $p \in R^2$  of vertex  $c$ , there is only one positive value, and the others are zeros. We first define a

low-resolution representation  $\bar{p} = \lfloor \bar{p}/R \rfloor$  with the downsampling stride  $R = 4$ , and then map each vertex to a Gaussian heatmap  $Y_{xy,c}$ . Also, when two Gaussian functions have overlapping areas, we take the maximum value of the heatmaps instead of the average. In this way, the close relationship to peak points can be preserved. The training object of vertex prediction is similar to focal loss  $L_{det}$  [26].

In the next section, we will introduce vertex matching to find the next vertex for each vertex.

#### 3.2. Vertex Matching

In the second stage, we perform a vertex matching task to determine whether a pair of vertexes are from the same lane line. This task is finally fed into two branches: classification and regression, which are designed to match vertexes for each lane line and predict the corrected location for each vertex, respectively. The overall process is illustrated in Figure 1.

For vertex  $v_i$ , we search its top-K neighboring vertexes according to Euclidean distance from  $v_i$  to other vertexes. Then we aggregate location representation and feature maps into a vector, which contains abundant vertex location and high-resolution semantic features. Specifically, we represent the segmentation map as  $\hat{Y}_{seg}$ ,  $T_{v_i} = \{m_{v_{ik}}\}_{k=1}^K$  represents top-K neighboring vertex maps of vertex  $v_i$ ,  $f_{v_i} \in R^{H \times W \times (C+K+2)}$  is the aggregated vector, and  $F \in R^{H \times W \times C}$  denotes the feature representation producing from the backbone. The  $f_{v_i}$  is generated by concatenating  $\hat{Y}_{seg}$ ,  $T_{v_i}$  and  $F$  together with vertex map of  $v_i$  on the channel dimension. To decrease the computational budget, we crop the  $f_{v_i}$  by a square with size  $S \times S$ , whose center is at the vertex  $v_i$ .  $\hat{f}_{v_i}$  representing the cropped aggregated vector.

The  $\hat{f}_{v_i}$  is finally fed into two branches: classification and regression, which are targeted to classify the next vertex of  $v_i$  from K neighboring vertexes and regress the corrected location of  $v_i$ , respectively. The classification head consists of a linear projection layer followed by a softmax function. We use the cross-entropy loss as the classification loss  $L_{cls}$  between true class map  $t_{v_i}$  and predicted confidence map  $\hat{t}_{v_i}$ .

The regression branch outputs are the location  $d(v_i) = (d_x(v_i), d_y(v_i))$  for vertex  $v_i$ .  $d_x(v_i)$  and  $d_y(v_i)$  denotes the prediction of the corrected coordinate of vertex  $v_i$ . The ground truth location of vertex  $v_i$  is represented as  $u(v_i) = (u_x(v_i), u_y(v_i))$ . We use smooth L1 loss as the location regression loss  $L_{reg}$ .

Finally, we employ a multi-task training strategy to minimize the objective loss, which comprises five parts: segmentation loss, vertex prediction loss, remapping offset loss, classification loss, and location regression loss. We formulate the objective loss as:

$$L = L_{seg} + L_{det} + \lambda_1 L_{cls} + \lambda_2 L_{reg} \quad (1)$$

where  $\lambda_1$  and  $\lambda_2$  are the regularization parameters. We empirically set them as 0.1 and 0.01 in our experiment.

Methods	Precision $\uparrow$			Recall $\uparrow$			F1-score $\uparrow$		
	2.0	5.0	10.0	2.0	5.0	10.0	2.0	5.0	10.0
Naive baseline	0.607	0.890	0.928	0.505	0.736	0.768	0.533	0.778	0.811
RoadTracer [20]	0.391	0.707	0.791	0.416	0.743	0.821	0.533	0.778	0.811
VecRoad [21]	0.461	0.769	0.854	0.459	0.752	0.830	0.458	0.756	0.837
DAGMapper [22]	0.407	0.751	0.868	0.353	0.649	0.747	0.371	0.684	0.787
iCurb [23]	0.550	0.833	0.890	0.538	0.815	0.873	0.542	0.820	0.910
AerialLaneNet	<b>0.692</b>	<b>0.925</b>	<b>0.941</b>	<b>0.613</b>	<b>0.879</b>	<b>0.920</b>	<b>0.613</b>	<b>0.876</b>	<b>0.964</b>

**Table 2. Quantitative comparison** against other methods designed for extracting vectorized map elements.

## 4. EXPERIMENTS

### 4.1. Implementation Details

Our AerialLaneNet takes as input  $1280 \times 1280$  resolution patches randomly cropped from the raw images with random flips. The network is trained with Adam optimizer and cosine annealing schedule with the initial learning rate of  $1e - 3$ , a momentum of 0.9 and train the network for 100 epochs, which we drop by a factor of 5 at epoch 40 and 60. We adopt a batch size of 4 for each round. Training the network took around 16 hours. To train the Inception network that reasons about whether a connection in the graph exists. For the segmentation and feature extraction stage, we adopt HRNet [24] as the backbone, and for next vertex prediction we exploit a ResNet-50 as the classifier.

K	F1-Score <sub>class</sub>	MSE <sub>position</sub>	Runtime <sub>class</sub>
5	80.2	10.2	0.03
10	81.7	8.8	0.05
20	83.8	7.4	0.10
40	84.0	5.2	0.16

**Table 3. Ablation** on K number of vertex candidate.

### 4.2. Results and Comparisons

Table 2 presents the performance of AerialLaneNet outperforms all other methods by a considerable margin and our method excel in Precision, Recall and F1-score under different thresholds, demonstrating the effectiveness and robustness of our proposed architecture. We also provide qualitative evaluation in the form of visualization results. Figure 3 shows the original image, ground truth lanes and vertices and our prediction results. Our method connected most of the vertices correctly and restored the lane topology correctly from vertices, thus successfully predicting the main structure of lanes. However, due to the shift of vertices location prediction, our predicted lanes sometimes warp compared to the ground truth.

We conduct an ablation study on the number of candidates in the next vertex prediction process. We test several K values, and the results are shown in Table 3. We found that with the increasing number of K, the final MSE of the next vertex position regression significantly drop down, indicating a bet-

ter prediction on next vertex position. The F1-Score of classifying the next vertex increases as well. However, the runtime increases linearly, due to the extra burden of classification.

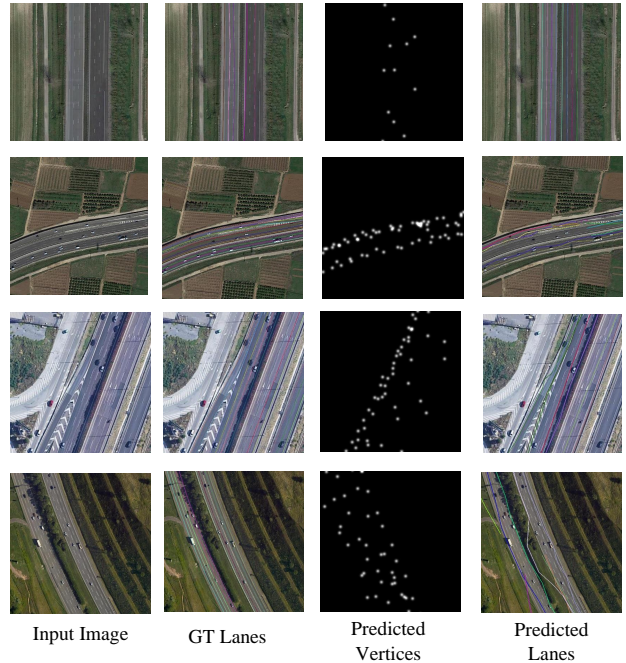


**Fig. 3.** The ground truth and baseline experimental results. Fig.3 (a) is the image patch, and Fig.3 (b) is the lane mask generated from polyline annotation. Our dataset consists of high-resolution images, with typical lane widths larger than 5 pixels and minimal occlusion, making lane detection achievable.

## 5. CONCLUSION

In this paper, we propose a dataset consisting of aerial images with various backgrounds and fine-grained lane types, which will be made publicly available upon publication of this paper. Furthermore, we introduce a baseline method, AerialLaneNet, for detecting lane lines using aerial images. Extensive experiments confirm that the proposed method consistently outperforms state-of-the-art methods, and our study can be utilized in online automatic mapping, enabling autonomous driving and intelligent transportation applications.

## 6. REFERENCES

- [1] Dapeng Li, Zhiwei Xu, Bin Zhang, and Guoliang Fan, “From explicit communication to tacit cooperation: A novel paradigm for cooperative marl,” *arXiv preprint arXiv:2304.14656*, 2023.
- [2] Ting Liu, Wansen Wu, Yue Hu, Youkai Wang, Kai Xu, and Quanjun Yin, “Prompt-based context-and domain-aware pretraining for vision and language navigation,” *arXiv preprint arXiv:2309.03661*, 2023.
- [3] Dapeng Li, Feiyang Pan, Jia He, Zhiwei Xu, Dandan Tu, and Guoliang Fan, “Style miner: Find significant and stable explanatory factors in time series with constrained reinforcement learning,” *arXiv preprint arXiv:2303.11716*, 2023.
- [4] Ting Liu, Yue Hu, Wansen Wu, Youkai Wang, Kai Xu, and Quanjun Yin, “Dap: Domain-aware prompt learning for vision-and-language navigation,” *arXiv preprint arXiv:2311.17812*, 2023.
- [5] Farzeen Munir, Shoaib Azam, et al., “Autonomous vehicle: The architecture aspect of self driving car,” in *Proceedings of the 2018 International Conference on Sensors, Signal and Image Processing*, 2018, pp. 1–5.
- [6] Jiawei Yao and Jusheng Zhang, “Depthssc: Depth-spatial alignment and dynamic voxel resolution for monocular 3d semantic scene completion,” *arXiv preprint arXiv:2311.17084*, 2023.
- [7] Jiawei Yao, Chuming Li, Keqiang Sun, Yingjie Cai, Hao Li, Wanli Ouyang, and Hongsheng Li, “Ndc-scene: Boost monocular 3d semantic scene completion in normalized device coordinates space,” in *Proceedings of the IEEE/CVF International Conference on Computer Vision*, 2023, pp. 9455–9465.
- [8] Jiawei Yao, Chen Wang, Tong Wu, and Chuming Li, “Geometry-guided ray augmentation for neural surface reconstruction with sparse views,” *arXiv preprint arXiv:2310.05483*, 2023.
- [9] Jiawei Yao and Yingxin Lai, “Dynamicbev: Leveraging dynamic queries and temporal context for 3d object detection,” *arXiv preprint arXiv:2310.05989*, 2023.
- [10] Jiawei Yao, Tong Wu, and Xiaofeng Zhang, “Improving depth gradient continuity in transformers: A comparative study on monocular depth estimation with cnn,” *arXiv preprint arXiv:2308.08333*, 2023.
- [11] Bencheng Liao, Shaoyu Chen, Wang, et al., “Maptr: Structured modeling and learning for online vectorized hd map construction,” *arXiv preprint arXiv:2208.14437*, 2022.
- [12] Bo Jiang, Shaoyu Chen, Xu, et al., “Vad: Vectorized scene representation for efficient autonomous driving,” *arXiv preprint arXiv:2303.12077*, 2023.
- [13] Qi Li, Yue Wang, Yilun Wang, and Hang Zhao, “Hdmapnet: An online hd map construction and evaluation framework,” in *ICRA*. IEEE, 2022, pp. 4628–4634.
- [14] Zhenhua Xu, Yuxuan Liu, et al., “Rngdet: Road network graph detection by transformer in aerial images,” *IEEE Transactions on Geoscience and Remote Sensing*, vol. 60, pp. 1–12, 2022.
- [15] Dongkwon Jin, Wonhui Park, et al., “Eigenlanes: Data-driven lane descriptors for structurally diverse lanes,” in *CVPR*, 2022, pp. 17163–17171.
- [16] Fan Yan, Ming Nie, et al., “Once-3dlanes: Building monocular 3d lane detection,” in *CVPR*, 2022, pp. 17143–17152.
- [17] Li Chen, Chonghao Sima, et al., “Persformer: 3d lane detection via perspective transformer and the openlane benchmark,” in *ECCV*, 2022.
- [18] “Google maps,” <https://developers.google.com/maps>.
- [19] “Qgis,” <https://www.qgis.org/en/site/>.
- [20] Favien Bastani, Songtao He, et al., “Roadtracer: Automatic extraction of road networks from aerial images,” in *CVPR*, 2018, pp. 4720–4728.
- [21] Yong-Qiang Tan, Shang-Hua Gao, et al., “Vecroad: Point-based iterative graph exploration for road graphs extraction,” in *CVPR*, 2020, pp. 8910–8918.
- [22] Namdar Homayounfar, Wei-Chiu Ma, et al., “Dagmapper: Learning to map by discovering lane topology,” in *ICCV*, 2019, pp. 2911–2920.
- [23] Zhenhua Xu, Yuxiang Sun, and Ming Liu, “icurb: Imitation learning-based detection of road curbs using aerial images for autonomous driving,” *IEEE Robotics and Automation Letters*, vol. 6, no. 2, pp. 1097–1104, 2021.
- [24] Jingdong Wang, Ke Sun, Cheng, et al., “Deep high-resolution representation learning for visual recognition,” *IEEE transactions on pattern analysis and machine intelligence*, vol. 43, no. 10, pp. 3349–3364, 2020.
- [25] Hei Law and Jia Deng, “Cornernet: Detecting objects as paired keypoints,” in *ECCV*, 2018, pp. 734–750.
- [26] Tsung-Yi Lin, Priya Goyal, Ross Girshick, Kaiming He, and Piotr Dollár, “Focal loss for dense object detection,” in *ICCV*, 2017, pp. 2980–2988.